JVI Journals.ASM.org

Temporal Characterization of Marburg Virus Angola Infection following Aerosol Challenge in Rhesus Macaques

Kenny L. Lin,[a] Nancy A. Twenhafel,[a] John H. Connor,[b] Kathleen A. Cashman,[a] Joshua D. Shamblin,[a] Ginger C. Donnelly,[a] Heather L. Esham,[a] Carly B. Wlazlowski,[a] Joshua C. Johnson,[a,c] Anna N. Honko,[a,c] Miriam A. Botto,[a] Judy Yen,[b] Lisa E. Hensley,[a,c] Arthur J. Goff[a]

United States Army Medical Research Institute of Infectious Diseases, Fort Detrick, Maryland, USA[a]; Boston University School of Medicine and National Emerging Infectious Diseases Laboratory, Boston, Massachusetts, USA[b]; Integrated Research Facility, National Institute of Allergy and Infectious Diseases, Fort Detrick, Maryland, USA[c]

ABSTRACT

Marburg virus (MARV) infection is a lethal hemorrhagic fever for which no licensed vaccines or therapeutics are available. Development of appropriate medical countermeasures requires a thorough understanding of the interaction between the host and the pathogen and the resulting disease course. In this study, 15 rhesus macaques were sequentially sacrificed following aerosol exposure to the MARV variant Angola, with longitudinal changes in physiology, immunology, and histopathology used to assess disease progression. Immunohistochemical evidence of infection and resulting histopathological changes were identified as early as day 3 postexposure (p.e.). The appearance of fever in infected animals coincided with the detection of serum viremia and plasma viral genomes on day 4 p.e. High (>10^7 PFU/ml) viral loads were detected in all major organs (lung, liver, spleen, kidney, brain, etc.) beginning day 6 p.e. Clinical pathology findings included coagulopathy, leukocytosis, and profound liver destruction as indicated by elevated liver transaminases, azotemia, and hypoalbuminemia. Altered cytokine expression in response to infection included early increases in Th2 cytokines such as interleukin 10 (IL-10) and IL-5 and late-stage increases in Th1 cytokines such as IL-2, IL-15, and granulocyte-macrophage colony-stimulating factor (GM-CSF). This study provides a longitudinal examination of clinical disease of aerosol MARV Angola infection in the rhesus macaque model.

IMPORTANCE

In this study, we carefully analyzed the timeline of Marburg virus infection in nonhuman primates in order to provide a well-characterized model of disease progression following aerosol exposure.

Marburg virus (MARV) is a single-stranded negative-sense RNA virus that belongs to the family *Filoviridae* (1). The genus *Marburgvirus* is composed of a single species, *Marburg marburgvirus*, which includes the subspecies MARV and Ravn virus. The first outbreak of MARV occurred simultaneously in Germany and the former Yugoslavia in August 1967, when laboratory personnel were exposed to the virus through contact with infected tissues from African green monkeys imported from Uganda (2, 3). Seven of the 32 confirmed human cases (mostly primary exposures) succumbed to infection (4, 5). From 1975 to 1998, subsequent MARV infections were limited to sporadic cases in selected areas of Africa, until the occurrence of two large outbreaks in the Democratic Republic of the Congo from 1998 to 2000 and Angola from 2004 to 2005 (6, 7). The case fatality rates for these outbreaks were 83% (128/154) and 90% (227/252), respectively, and established MARV disease as an important public health threat (8, 9).

There are currently no licensed medical countermeasures to combat infections with filoviruses such as MARV. Due to the high pathogenicity of MARV, it is classified as a biological select agent by the U.S. Department of Health and Human Services (HHS) and a category A bioterrorism agent by the Centers for Disease Control and Prevention (CDC) (1). As such, any MARV research must be conducted in highly regulated biosafety level 4 (BSL-4) containment laboratories.

Data from the ongoing Ebola virus (EBOV) outbreak in Western Africa have suggested that filoviruses have the potential to be transmitted by airborne droplets, highlighting the need to study the disease course following aerosol exposure. It has also been demonstrated that Ebola can be transmitted from pigs to nonhuman primates when they are cohoused (10). While the respiratory route of infection may not be the primary means of filovirus transmission, the virus can be spread by contact with large droplets containing virus (i.e., a sneeze). Moreover, there are continual concerns over a potential bioterrorist attack. It was previously thought that filoviruses would not remain viable for long in an uncontrolled environment if there was ever a purposeful release. However, both EBOV and MARV can be detected for up to 90 min in a dynamic aerosol spray (11).

Well-characterized animal models of infection are critical to the development of vaccines and antiviral compounds that protect against MARV infection (12). A number of MARV studies have been conducted using various exposure routes, doses, virus strains (Ci67, Angola, and Musoke), and animal models (mice, guinea pigs, Syrian golden hamsters, and nonhuman primates [NHP])

Received 5 May 2015 **Accepted** 10 July 2015

Accepted manuscript posted online 22 July 2015

Citation Lin KL, Twenhafel NA, Connor JH, Cashman KA, Shamblin JD, Donnelly GC, Esham HL, Wlazlowski CB, Johnson JC, Honko AN, Botto MA, Yen J, Hensley LE, Goff AJ. 2015. Temporal characterization of Marburg virus Angola infection following aerosol challenge in rhesus macaques. J Virol 89:9875–9885. doi:10.1128/JVI.01147-15.

Editor: D. S. Lyles

Address correspondence to Arthur J. Goff, arthur.j.goff.civ@mail.mil.

doi:10.1128/JVI.01147-15

(3, 13–19). From these tests, nonhuman primate models in cynomolgus or rhesus macaques most accurately recapitulate the clinical aspects of Marburg virus disease (MVD) observed in human infections (14).

The aim of this work was to provide a well-defined animal model of aerosolized MARV Angola infection for the use in future vaccine and therapeutic assessment studies. We report the findings of a sequential sacrifice study of 15 rhesus macaques exposed to aerosolized MARV Angola variant Ang1379c. Disease progression was evaluated based on clinical parameters, virology, serology, inflammatory responses, gross necropsy, histopathology, and immunohistochemistry. Assessment of these parameters at 2-day intervals provided valuable insight into not only the timeline of viral dissemination but also immunological changes in response to infection, as reported in the accompanying article (20). Our results demonstrate that the disease caused by Marburg virus delivered by the aerosol route is similar to disease resulting from intramuscular exposure.

TABLE 1 Sacrifice and bleed days and actual delivered dose

NHP cage	MARV delivered dose (PFU)	Bleed time(s) PE[a]	Sacrifice day
1	3.86×10^3	6 h	1
2	3.98×10^3	6 h	1
3	4.93×10^3	6 h	1
4	4.91×10^3	6 h, 2	3
5	5.95×10^3	2	3
6	3.67×10^3	2	3
7	4.75×10^3	6 h, 1	5
8	3.48×10^3	1	5
9	3.09×10^3	1	5
10	5.40×10^3	2, 4	7
11	3.39×10^3	4	7
12	6.25×10^3	4	7
13	3.76×10^3	3, 6, 8	8
14	3.43×10^3	3, 6, 8	9
15	4.67×10^3	6, 8	9

[a] In days, unless otherwise specified.

MATERIALS AND METHODS

Animals. Research was conducted under an IACUC approved protocol in compliance with the Animal Welfare Act, PHS Policy, and other federal statutes and regulations relating to animals and experiments involving animals. The facility where this research was conducted is accredited by the Association for Assessment and Accreditation of Laboratory Animal Care, International and adheres to principles stated in the *Guide for the Care and Use of Laboratory Animals* (21). Fifteen healthy, adult rhesus macaques (*Macaca mulatta*) weighing between 5 and 9 kg were obtained from World Wide Primates (Miami, FL). Prior to the start of study, the animals were acclimated to a BSL-4 laboratory. The animals were found to be negative for standard viral agents (herpesvirus B, simian T-cell leukemia virus 1 [STLV-1], simian immunodeficiency virus [SIV], and simian retrovirus 1 [SRV-1], -2, and -3) and were negative for filovirus antibodies. NHPs were randomized to five groups of 3 animals each using Excel (Microsoft, Redmond, WA), with one group of animals to be sacrificed on each of the following days: 1, 3, 5, 7, and 9 postexposure (p.e.). On days −8 and −7 prior to infection, animals received a physical examination, including body weight determination, rectal temperature determination, and clinical observations. Baseline parameters for hematology, serum chemistry, coagulation, and cytokine expression were also obtained on these days. The data in the figures are the average for all of the NHPs that samples were obtained from at that time point. Standard deviations of those data points are also shown.

Virus. The MARV Angola isolate used for this study was from a patient specimen collected in 2005 (Marburg virus H.sapiens-tc/ANG/2005/Angola-1379c [order *Mononegavirales*, family *Filoviridae*, species *Marburg marburgvirus*]) (7). The reference sequence, Ang1379c, was determined from RNA isolated directly from clinical material and also from the virus isolate (Ang1379v) after one passage on Vero E6 cells. A sample was obtained from the Centers for Disease Control and Prevention, Atlanta, GA, USA, following two passages in VeroE6 cells. A virus seed stock (passage 3) was previously propagated in Vero E6 cells and analyzed for sterility, purity, and morphology using electron microscopy, real-time PCR, and tests for endotoxin and mycoplasma. Nucleotide sequencing was conducted on the seed stock, and plaque assay was used to determine the final virus concentration.

Aerosol exposure. Animals were exposed to a small-particle aerosol target dose of 1,000 PFU of MARV Angola on day 0 using the U.S. Army Medical Research Institute of Infectious Diseases (USAMRIID) head-only automated bioaerosol exposure system (ABES-II). Prior to exposure, each animal was anesthetized by intramuscular injection of tiletamine hydrochloride/zolazepam hydrochloride (Telazol; 3 mg/kg of body weight; Fort Dodge Laboratories, Fort Dodge, IA). A full-body plethysmograph (Buxco Research Systems, Wilmington, NC) was used to ascertain each animal's respiratory rate and capacity. The animal was then placed in the ABES-II for the exposure time calculated based on that individual animal's plethysmograph data. The aerosol dose was calculated by multiplying the volume of inhaled exposure material (length of exposure × respiratory minute volume) by concentration of virus in the aerosol. Using a Collison nebulizer (BGI Inc., Waltham, MA), a target aerosol 1 to 3 μm in diameter was generated. Hanks' buffered saline with 1% fetal calf serum and 0.001% antifoam A was used in an all-glass impinger (AGI; Ace Glass, Vineland, NJ) to collect a sample of aerosolized virus during exposure. Starting virus concentrations and exposure dose (AGI material) (Table 1) were confirmed through plaque assay.

Postexposure monitoring. A group of animals ($n = 3$) was euthanized on each of the following days: 1, 3, 5, and 7 p.e. One animal succumbed on day 8 p.e., and the remaining two were sacrificed on day 9 p.e. To ensure that hematological, serological, and physiological data were available for each day of the study (days when euthanasia was not scheduled), physical examinations and blood collection were also performed for selected surviving animals on days 2, 4, 6, and 8 p.e. At the time of euthanasia, body weight and rectal temperature were determined and blood collection was performed for each animal.

Necropsy. Following euthanasia, a complete necropsy was conducted on each animal in a BSL-4 laboratory. The following tissues were collected from each animal for viral genome, viral titer analysis, and histopathology: axillary lymph node (LN), inguinal LN, mandibular LN, mesenteric LN, tracheobronchial LN, lung, liver, spleen, brain, kidney, bone marrow, heart, adrenal gland, pancreas, and ovary. Tissues were fixed by immersion in containers of 10% neutral buffered formalin for a minimum of 21 days for histopathologic examination.

Histology and molecular pathology. Following fixation, tissue samples were embedded in paraffin sections and further analyzed for immunohistochemistry (IHC), histology, and TUNEL staining. TUNEL staining was assessed using an ApopTag *in situ* apoptosis detection kit (Millipore Corporation, Billerica, MA) as per the manufacturer's protocol, as previously reported (13). IHC was performed using an immunoperoxidase kit EnVision system (Dako Inc, Carpinteria, CA) according to the manufacturer's protocol. Anti-MARV GP Angola antibody (USAMRIID) and caspase 3 antibody (Cell Signaling Technology, Beverly, MA) labeling was performed as previously described (13). Histology sections were stained with hematoxylin and eosin.

Serum chemistry, hematology, and coagulation tests. Whole blood was collected in serum clot activator Vacuette tubes (Greiner Bio-One, Monroe, NC) for serum separation. Serum tubes were allowed to clot for a minimum of 30 min and centrifuged at 1,800 × *g* for 10 min at an ambient temperature. Serum was separated within 1 h of collection and

analyzed on a Piccolo point-of-care blood analyzer (Abaxis, Union City, CA) using a Piccolo Chem13 panel disc. The parameters examined included creatinine (CRE), blood urea nitrogen (BUN), albumin, total protein, aspartate aminotransferase (AST), and alanine aminotransferase (ALT).

Whole blood was also collected in tripotassium EDTA-coated Vacuette tubes (Greiner Bio-One, Monroe, NC) for hematological analysis. Complete blood count analysis was performed on whole blood within 4 h of blood collection using a HemaVet 950FS hematology analyzer (Drew Scientific, Oxford, CT). The parameters analyzed included white blood cell counts, neutrophil counts, lymphocyte counts, red blood cell counts, percent hematocrit, and platelet counts.

Coagulation abnormalities and presence of D-dimers were assessed on plasma separated from whole blood. The coagulation parameters activated partial thromboplastin time (aPTT) and prothrombin time (PT) were determined using a ThromboScreen (Fischer Diagnostics, Middletown, VA) per the manufacturer's protocol. D-dimers were analyzed using an Asserachrom D-dimer enzyme immunoassay kit (Diagnostica Stago Inc., Troy Hills, NJ). Samples were read on a Spectramax M5 microplate reader (Molecular Devices, Sunnyvale, CA) with Softmax Pro 4.7 software (Molecular Devices).

Peripheral blood mononuclear cells (PBMCs) were isolated from whole blood using Histopaque-1077 prefilled Accuspin tubes (Sigma-Aldrich, St. Louis, MO). Total cell counts and percent cell viability were determined using trypan blue staining solution and a Countess automated cell counter (Life Technologies, Grand Island, NY). After cells were counted, 250 μl of viable cells was mixed with 750 μl of TRI Reagent LS (Sigma-Aldrich, St. Louis, MO) and stored at −70 ± 10°C.

Plaque assay. Viral load was determined from plaque assays performed on the viral seed stock, the virus challenge working stock, samples of aerosol exposure (via AGI), serum samples, and tissues collected at necropsy. Tissues were homogenized in 500 μl of cell culture medium with a Tissuelyser II (Qiagen, Valencia, CA) at 30 Hz for 1 min. All experimental samples were serially diluted and plated in duplicate onto confluent Vero E6 cells in 6-well plates. Following 45 to 60 min of initial absorption (without cell culture media), 2 ml of 1× Avicel overlay (2.5% preparation mixed 1 to 1 with 2× cell culture media) were added to each well and the plates incubated at 37°C and 5% CO_2. The plates were stained on day 7 with 1 ml of 0.4% crystal violet at room temperature. Plaques were counted on day 8.

Viral genome quantification. Viral RNA was quantified from plasma and tissues treated with EDTA collected at necropsy by quantitative reverse transcription-PCR (qRT-PCR) using an ABI 7500 Fast Dx (Life Technologies, Grand Island, NY). Plasma and homogenized tissue samples were inactivated with 1 part to 3 parts TRI Reagent LS (Sigma-Aldrich, St. Louis, MO) and stored at −70 ± 10°C. RNA was extracted using a QIAamp viral RNA minikit (Qiagen, Valencia, CA). qRT-PCR was performed utilizing a SuperScript II one-step RT-PCR system (Life Technologies, Grand Island, NY) with primers and probes specific for the MARV matrix (VP40) gene (forward primer, 5′-CCA GTT CCA GCA ATT ACA ATA CAT ACA-3′; reverse primer, 5′-GCA CCG TGG TCA GCA TAA GGA-3′; probe, CAA TAC CTT AAC CCC C-MGBNFQ [minor groove binder-tagged nonfluorescent quencher]). Samples were analyzed in triplicate; a PFU equivalent (PFU/ml eq) was calculated by taking the average of the reported concentration values and multiplying by the TRIzol extraction, the elution volumes, and the reaction volume. The calculations were standardized using an inactivated viral stock of known concentration which was extracted, eluted, and analyzed identically to the samples to generate a standard curve (22).

Cytokine analysis by multiplex antibody bead assay. Previously frozen plasma samples were thawed and assayed for protein cytokine and chemokine concentrations using a Millipore 23-plex NHP cytokine kit (EMD Millipore Corporation, Billerica, MA) with a Bio-plex analyzer (Bio-Rad, Hercules, CA). Standard curves were optimized using Bio-plex Manager 5.0 (Bio-Rad), and data were exported to Excel for analysis.

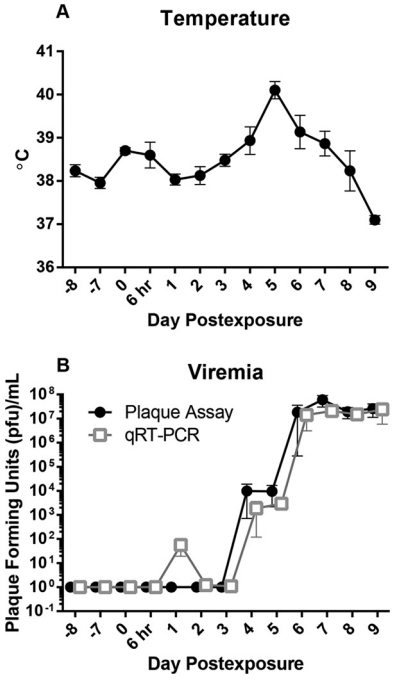

FIG 1 Body temperature and viremia. (A) Febrile illness as evidenced by changes in rectal body temperature. (B) Viremia was determined by plaque assay and qRT-PCR. qRT-PCR values are represented as PFU/ml equivalents calculated from viral genome copies. Each data point represents the average value for all samples that were analyzed at that time point.

RESULTS

To examine the course of disease following exposure of macaques to Marburg Angola virus through an aerosol route, 15 rhesus macaques were exposed to a target dose of 100 PFU by the aerosol route. The actual dose delivered ranged from 3.09×10^3 to 6.25×10^3 PFU (Table 1). Following exposure on day 0, one group of animals ($n = 3$) was sacrificed on days 1, 3, 5, and 7 postexposure (p.e.). One animal succumbed on day 8 p.e., and therefore only two were sacrificed on day 9 p.e. The animals that were alive on days 2, 4, 6, and 8 p.e. underwent physical examinations and phlebotomy.

Clinical signs of infection. The most common clinical findings following aerosol exposure to MARV included fever, lymphadenopathy, and maculopapular rash. Elevated body temperatures were noted beginning on day 4 p.e. and reached a peak of 40°C on day 5 p.e. (Fig. 1A). After the animals exhibited fever, general activity decreased, as well as food consumption. As the animals became moribund, a decline in body temperature to below baseline levels was observed by days 8 and 9 p.e. Moderate lymphadenopathy was present beginning on day 7 p.e., as evidenced by enlarged inguinal and axillary lymph nodes (5 to 10 mm in diameter) in 2 of the 6 remaining animals. The severity of lymphadenopathy was even more pronounced on days 8 and 9 p.e., with 2/3 animals displaying severe (11 to 20 mm in diameter) inguinal and axillary lymphadenopathy. A mild to moderate macular rash first appeared on day 7 p.e. in 2/3 animals and was present in all animals by days 8 and day 9 p.e. Other noteworthy clinical signs observed were severe edema of the hands, face, and feet, mild dehydration, and anorexia beginning day 7 p.e.

Virus replication. To assess the levels of infectious virus pres-

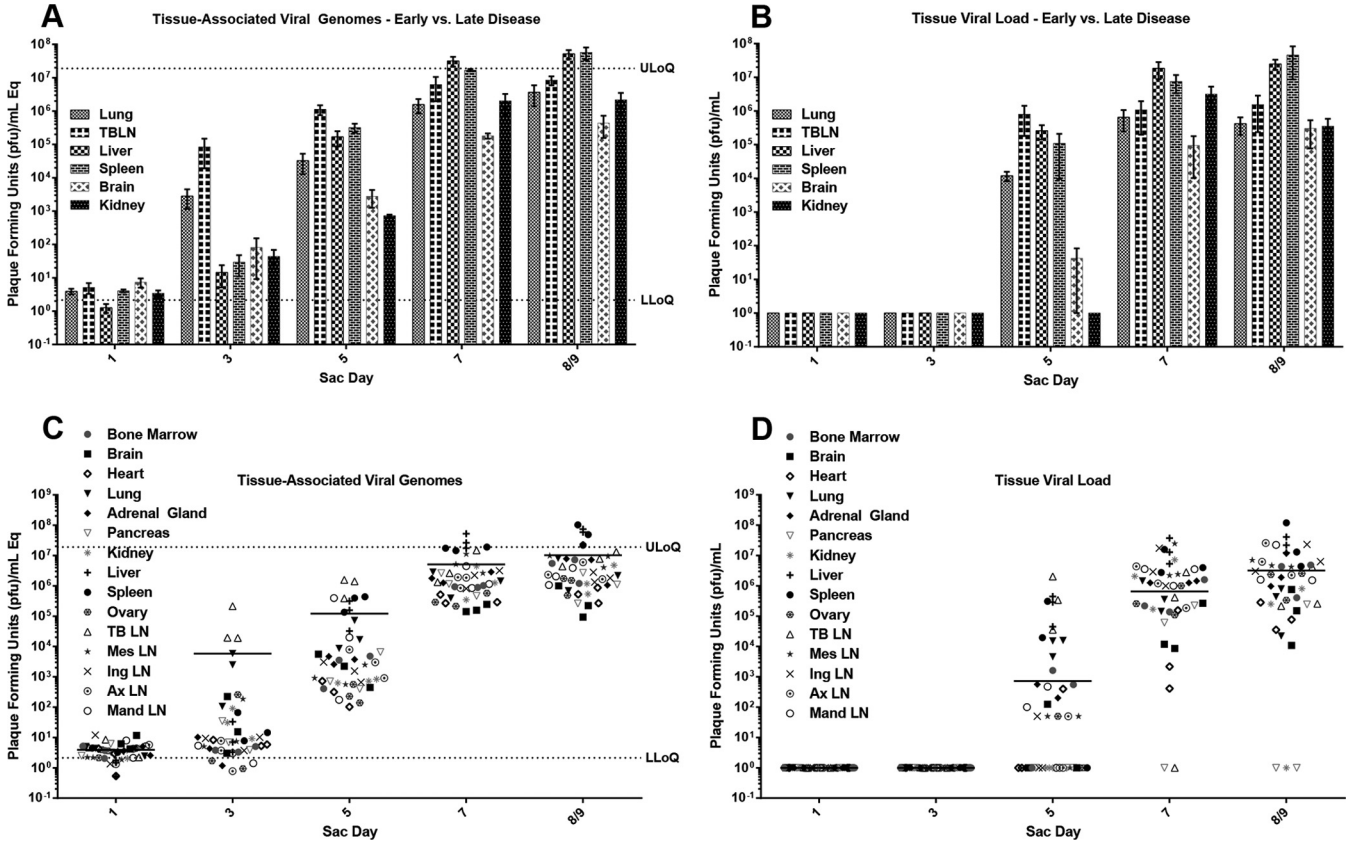

FIG 2 Tissue-associated MARV titers. Averaged tissue viral titers from qRT-PCR (PFU/ml equivalents calculated from viral genomes copies) (A) and averaged tissue viral titers from plaque assay per tissue type (B) demonstrate virus dissemination throughout MARV disease course. (C and D) Composites of all tissue-associated viral titers for each animal grouped by sacrifice day, as determined by qRT-PCR (C) and plaque assay (D). Ax, axillary; Ing, inguinal; LLoQ, lower limit of quantification; LN, lymph node; Mand, mandibular; Mes, mesenteric; TB, tracheobronchial; ULoQ, upper limit of quantification.

ent in circulation, viremia was determined by plaque assay using serum samples and reported as PFU/ml. Alternatively, viral load, or the presence of viral genomes, was determined by quantitative reverse transcriptase PCR (qRT-PCR) using plasma samples and reported as PFU/ml equivalent (eq) (Fig. 1B). Viremia was noted on day 4 p.e., with mean values of 9.87×10^3 PFU/ml by plaque assay and 1.87×10^3 PFU/ml eq by qRT-PCR. Peak viral titers were observed on day 7 p.e., with means of 5.97×10^7 PFU by plaque assay and 2.04×10^7 PFU eq by qRT-PCR (Fig. 1B).

Tissue-associated virus levels were determined through qRT-PCR (Fig. 2A and C) and plaque assay (Fig. 2B and D), respectively. Infectious virus was not detected in any tissue sample until day 5 p.e. (Fig. 2B); however, viral genomes were detected above the lower limit of quantification on day 3 p.e. in the lungs (2.83×10^3 PFU/ml eq) and tracheobronchial lymph nodes (8.42×10^4 PFU/ml eq) (Fig. 2A). At day 5 p.e., virus was detected in the liver (1.69×10^5 PFU/ml eq, 2.60×10^5 PFU/ml) and spleen (3.23×10^5 PFU/ml eq, 1.11×10^5 PFU/ml). By days 7 to 9 p.e., high viral loads were present in all tissues examined.

Host response to infection. Evidence of coagulopathy was present as early as day 4 p.e., with elevated prothrombin time (PT) and activated partial thromboplastin time (aPTT) observed on days 4 and 5 p.e. (Fig. 3B). This was accompanied by a reduction in platelets beginning on day 5 p.e. (Fig. 3A), as well as a rapid increase in D-dimers beginning on day 6 p.e. (Fig. 3C). Red blood cell counts and percent hematocrit (Fig. 3D) remained relatively unchanged throughout the study, except for an increase in both parameters noted on day 7 p.e. Taken together, these data suggest a rapid development of coagulation deficiencies that are hallmarks of filovirus infection.

No changes were observed in complete blood count (CBC) parameters until days 7 and 8 p.e. On day 7 p.e., there was an increase in white blood cells (leukocytosis) accompanied by neutrophilia (Fig. 3E and F). Elevated levels of creatinine and blood urea nitrogen beginning on day 8 p.e. were indicative of azotemia (Fig. 4A and B). We also observed a decrease in total protein and albumin concentrations on day 7 p.e. (Fig. 4C), as well as an increase in aspartate transaminase (AST) and alanine transaminase (ALT) on day 6 p.e. (Fig. 4D), suggestive of widespread organ damage.

To assess the immunological response to aerosol MARV infection, cytokine expression was analyzed using longitudinal serum samples. Concentrations of the Th2 cytokines interleukin 5 (IL-5) and IL-10 began to increase on days 3 to 4 p.e. While expression of IL-5 peaked on day 3 p.e., IL-10 did not reach peak expression until day 9 p.e. (data not shown) (20). Accumulation of Th1 cytokines in the serum was delayed compared to the Th2 cytokines. Increased expression of IL-2, IL-15, and tumor necrosis factor alpha (TNF-α) was not observed until days 4 to 5 p.e. (Fig. 5). The Th1 cytokines IL-6, gamma interferon (IFN-γ), and IL-18, along

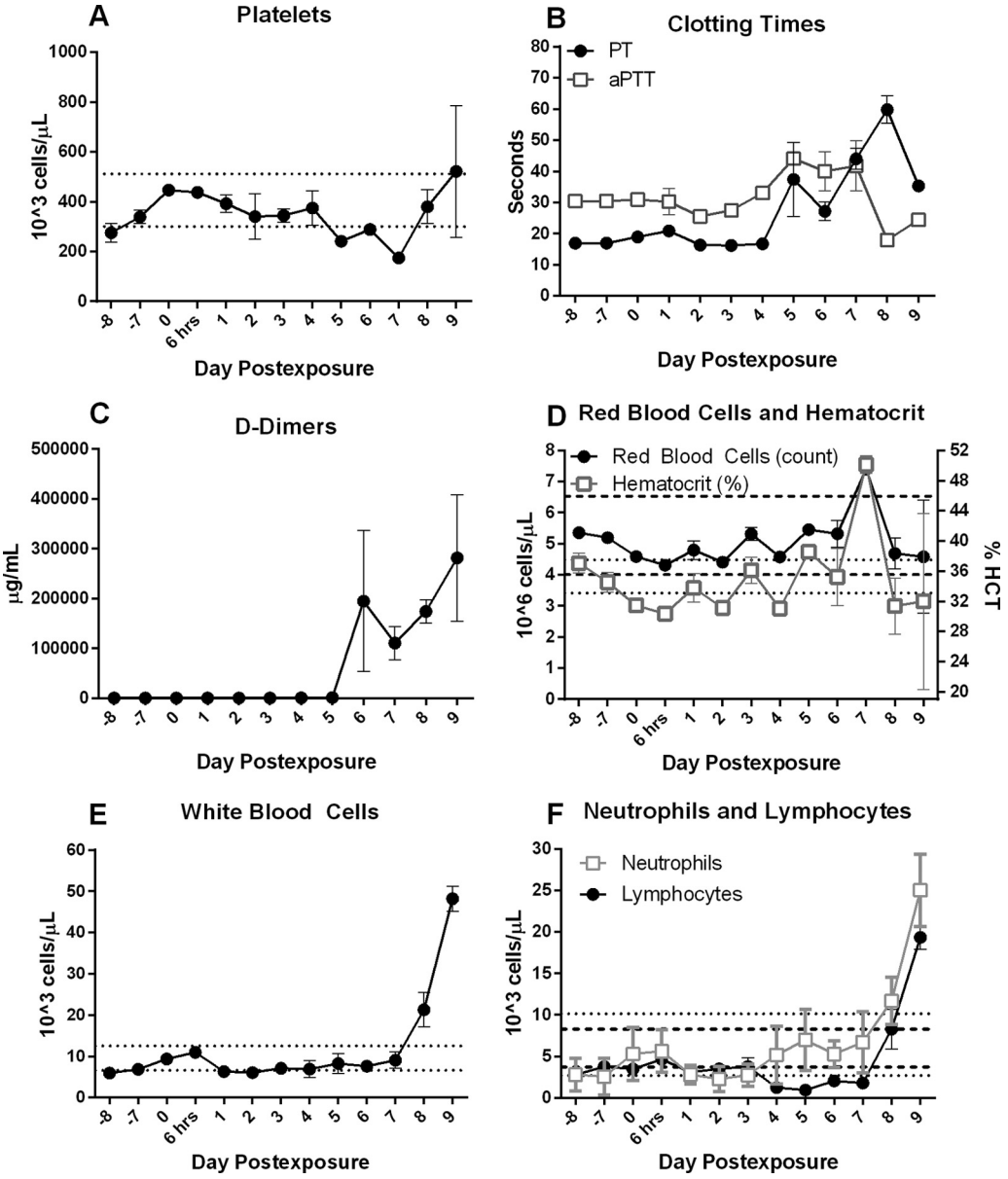

FIG 3 Hematology and coagulation profiles. Platelet deregulation (A), increases in clotting times (B), and the presence of D-dimers (C) illustrate a disruption in normal coagulation function. (D) Red blood cell and hematocrit remained relatively normal throughout the study, with increases attributed to splenic contraction and whole-body dehydration. Increasing total white blood cell counts (E) and neutrophil and lymphocyte counts (F) demonstrate progressive leukocytosis and lymphocytosis. Dashed lines represent ranges for RBC and lymphocytes on respective graphs. Dotted lines represent range values for hematocrit and neutrophils on respective graphs. Each data point represents the average value for all samples that were analyzed at that time point.

with the chemokines granulocyte macrophage-colony-stimulating factor (GM-CSF), macrophage inflammatory protein 1α (MIP-1α), and monocyte chemoattractant protein 1 (MCP-1), were the last to appear and increased in expression between days 6 and 9 p.e.

This cytokine/chemokine expression pattern was also seen at the transcriptome level in RNA isolated from PBMCs. Microarray analysis showed an increase in gene expression of Th2 cytokines IL-10, IL-4, and IL-5 on day 3 p.e. (20), with changes in the expression of Th1 cytokine IL-6 and the chemokines MCP-1 and MIP-1α observed in late-stage disease (day 7 p.e.) These results suggest that upregulation of Th2 cytokines occurs in the early stages of MARV infection, while upregulation of Th1 cytokines does not occur until the middle to late stages of disease.

Full necropsies were performed on all animals following euthanasia,. Enlarged tracheobronchial (TB) lymph nodes (Fig. 6A and B) were first evident on day 3 p.e. (1/3 animals) and present in all animals (9/9) euthanized on days 5, 7, 8, and 9 p.e. An enlarged and firm spleen first appeared on day 5 p.e. in 1/3 animals and was present in all animals euthanized on days 8 and 9 p.e. Noncollapsing (edematous) lung lobes were observed in all animals (9/9) beginning on day 5 p.e. Pale yellow and friable liver was observed in all animals (6/6) on days 7, 8, and 9 p.e. (Fig. 6F and G), while pale kidneys were observed on days 7 (2/3 animals) and 8/9 p.e.

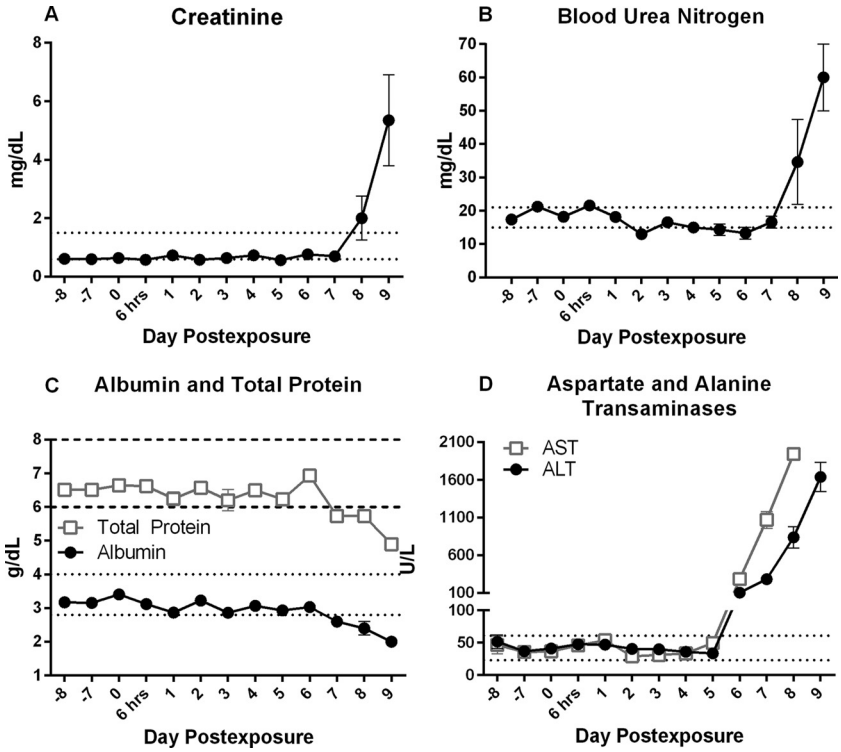

FIG 4 Clinical chemistry. Increased concentrations of creatinine (A) and blood urea nitrogen (B) confirm azotemia. A drop in total protein and albumin concentrations (C), along with increases in aspartate transaminase (AST) and alanine transaminase (ALT) (D), are associated with liver damage. Dashed and dotted lines represent normal range values. Each data point represents the average value for all samples that were analyzed at that time point.

(1/3 animals). The macular rash first observed during physical examinations was also present at the time of necropsy (Fig. 7D).

Histopathology and immunohistochemistry. Notable histologic changes following aerosol exposure to MARV Angola variant are detailed in Table 2, and immunohistochemistry results for MARV GP are listed in Table 3. The earliest signs of infection at the histology level were identified in the lymph nodes, particularly in those that drain the respiratory tract. Positive staining for MARV GP was present in the tracheobronchial lymph nodes beginning on day 3 p.e. Lymphocytosis was present within respiratory lymph nodes (tracheobronchial and mediastinal) beginning on day 3 p.e., larynx-associated lymphoid tissue (LALT) beginning on day 5 p.e., and trachea-associated lymphoid tissue (TALT) and bronchus-associated lymphoid tissue (BALT) beginning on day 7 p.e. Infection of the respiratory lymph nodes was followed by massive influx of MAC387$^+$ alveolar macrophages into the lymph node sinuses beginning on day 3 to 5 p.e., resulting in sinus expansion (Fig. 6C and D). By day 5 p.e., expansion had progressed to necrotizing lymphadenitis with massive lymphocyte destruction (Fig. 6E). Massive loss of lymphocytes was noted in the germinal centers and B-cell regions of the tracheobronchial lymph nodes, as evidenced by positive staining for caspase 3 (Fig. 7G to N) and TUNEL (terminal deoxynucleotidyltransferase-mediated dUTP-biotin nick end labeling) (data not shown). Partial or complete loss of lymph node architecture, hemorrhage, fibrin, edema, fibrinoid vasculitis, and fibrin thromboemboli were present on days 7, 8, and 9 p.e.

In the lungs themselves, a mild to moderate increase in alveolar macrophages (alveolar histiocytosis) with few intrahistiocytic cytoplasmic inclusion bodies was observed. Some animals had interstitial edema and congestion that were partly attributed to euthanasia procedures, while several animals also demonstrated evidence of terminal interstitial pneumonia.

Positive staining for MARV GP was noted in the liver and spleen beginning on day 5 p.e. Initial changes within the liver included degeneration and necrosis of hepatocytes, with vacuolar changes and intracytoplasmic inclusion bodies. The severity of degenerative changes in affected hepatocytes increased progressively in the animals euthanized on days 7, 8, and 9 p.e. Although no histologic changes were observed in the spleen on day 5, immunohistochemical evidence of MARV infection was present. Histologic changes within the spleen were not present until day 7 p.e. and included lymphocytolysis of splenic white pulp, edema, fibrin, and many tingible body macrophages. Lymphocyte apoptosis was observed in the germinal centers and B-cell regions of the spleen, as evidenced by positive staining for caspase 3 (Fig. 7G to N) and TUNEL (data not shown). Congestion and/or hemorrhage was noted in the marginal zones of the spleen, while macrophages with intracytoplasmic inclusion bodies, necrotic debris, congestion, and fibrin were observed within the red pulp. Caspase 3 immunoreactivity and TUNEL staining in these tissues increased in intensity progressively in the animals that were euthanized on days 5, 7, 8, and 9 p.e.

Multisystemic fibrinoid, necrotizing vasculitis and perivasculitis were present on days 7, 8, and 9 p.e. in 5/6 animals. Most tissues contained vasculitis and perivasculitis on days 8 and 9 p.e., with the exception of the lungs (Fig. 7C). Macular rash of haired skin in the axillary and inguinal regions, face, and pinna consisted

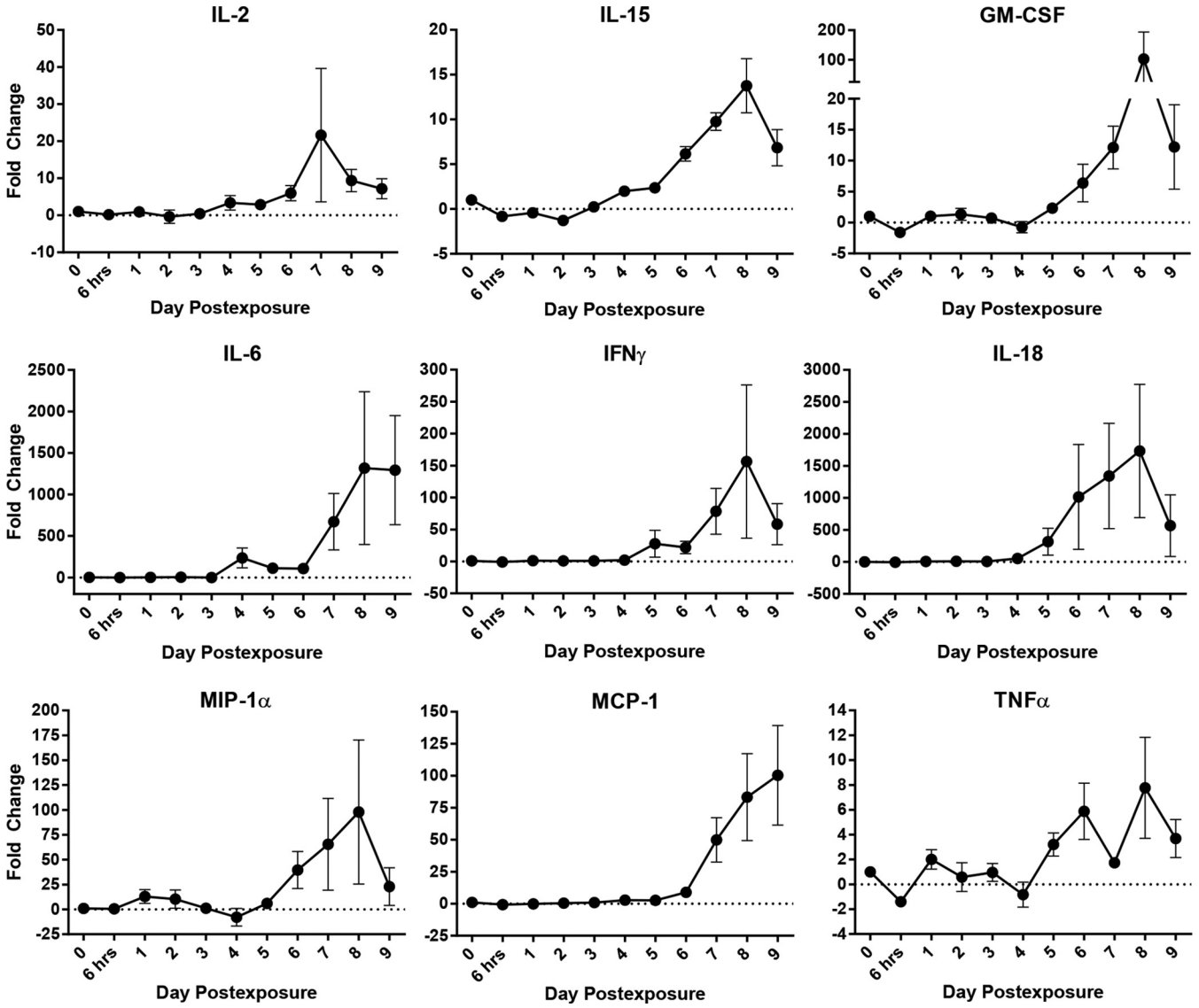

FIG 5 Cytokines and chemokines. Data are the change (fold) over baseline (dotted lines) for selected recruitment and proinflammatory cytokines and chemokines. Changes indicate a Th1 immune response late in disease. Each data point represents the average value for all samples that were analyzed at that time point.

solely of perivasculitis of superficial dermal blood vessels and congestion in the absence of hemorrhage or extravasation of red blood cells (Fig. 7E and F). Although skin sections were negative for expression of MARV antigen by IHC, macular rash is likely due to systemic MARV infection and the resulting widespread vasculitis. Vasculitis and perivasculitis of the kidneys were not accompanied by significant parenchymal or cellular changes, while the pale color of the kidneys was attributed to the lack of perfusion.

DISCUSSION

This study provides a detailed analysis of the rhesus macaque response to MARV exposure via the aerosol route. While MARV studies have been previously conducted in NHPs, these studies have been limited to terminal examination of Marburg virus-induced pathology. To our knowledge this is the first study to use serial sampling to create a detailed characterization of the development of MARV disease. In this experiment, the incubation period for MARV Angola appeared to be approximately 4 days, compared to a range of 5 to 14 days in humans. Early symptoms of MARV infection in humans include fever, headache, malaise, myalgia, and prostration. We also observed fever and decreased activity as well as inappetence early on in the disease course. During midstage disease, patients develop hemorrhagic manifestations, such as gastrointestinal mucosal petechiae and hemorrhage with bloody diarrhea, ecchymoses, and hematemesis. Progression to late stage disease is characterized by convulsions, dementia, severe coagulopathy, systemic shock, and multiorgan failure, often culminating in death (8, 23–25). The late-stage disease presentation in this model, as evidenced by high viral titers seen in the liver, spleen, and lymphoid tissues and by hematologic changes and coagulopathy, is comparable to the limited data that are available from patients infected with Marburg virus (3, 9, 24, 26, 27). This

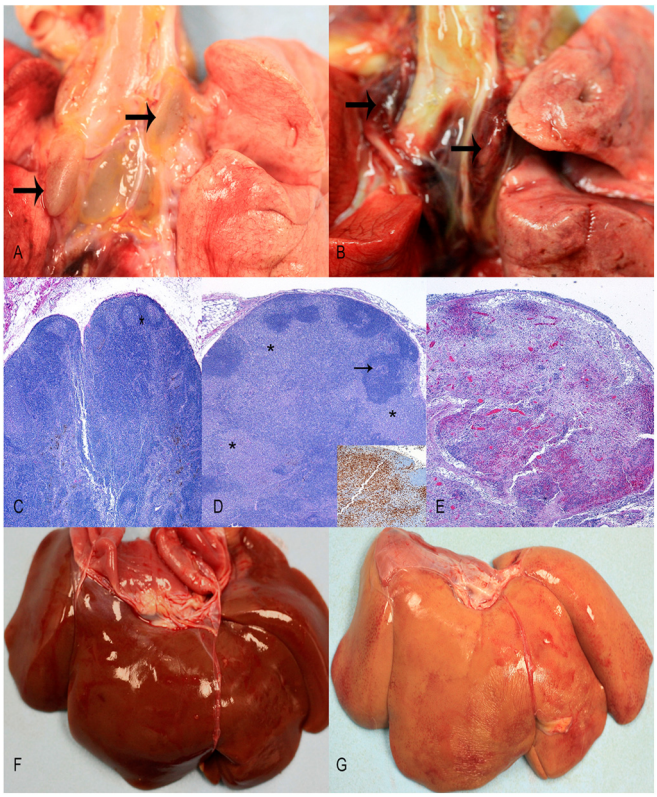

FIG 6 Pathology. (A) Gross pathology of tracheobronchial lymph nodes on day 3 p.e. (arrows) shows a mild increase in size and normal coloration. (B) Gross pathology image of tracheobronchial lymph nodes on day 9 p.e. (arrows) shows red to black (hemorrhage) discoloration and enlargement (approximately five times normal size). (C) Hematoxylin and eosin (HE) stain (magnification of ×100) of normal tracheobronchial lymph nodes on day 1 p.e. (D) HE stain (magnification of ×100) of tracheobronchial lymph node on day 3 p.e. shows sinuses (asterisks) that are severely expanded by a high number of macrophages, confirmed with anti-macrophage antibody 387 (MAC387) (inset), that surround and widely separate follicles (arrow). (E) HE stain (magnification of ×100) of tracheobronchial lymph nodes on day 9 p.e. demonstrates diffuse necrosis, edema, and hemorrhage. Gross liver images from days 1 (F) and 7 (G) p.e. show the dramatic change to yellow discoloration late in disease.

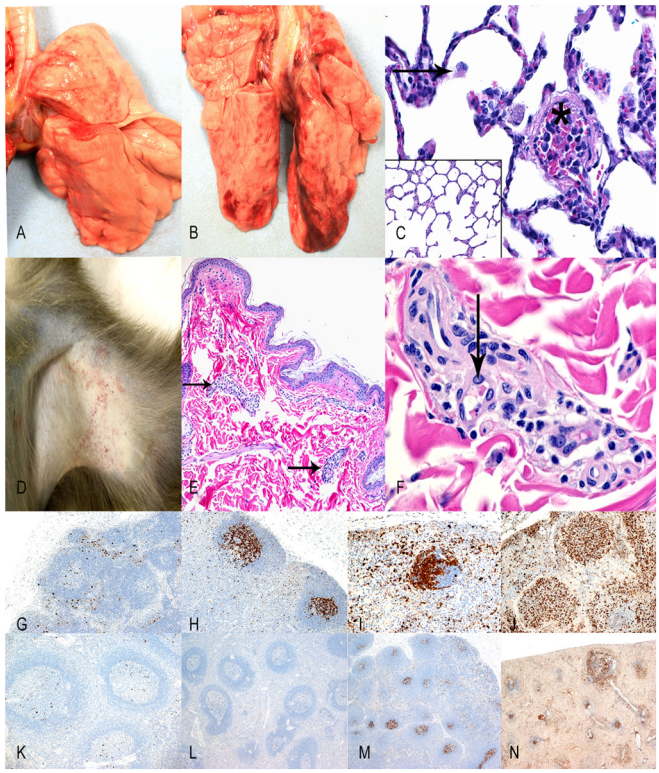

FIG 7 Pathology. No gross changes in the lungs are evident from day 1 p.e. (A) and day 9 p.e. (B). (C) HE stain of the lungs on day 9 p.e. (magnification of ×200) shows mild increases in alveolar histiocytes (arrow) and fibrin thromboemboli within blood vessels (asterisk) compared with normal day 1 p.e. lung (inset; 100× HE). (D) Axillary haired skin with mild macular rash day 9 p.e. (E) HE stain (magnification of ×100) of day 9 p.e. axillary haired skin that contains superficial blood vessels with perivascular inflammation (arrows) and no hemorrhage in the dermis. (F) Higher magnification (400× HE) of superficial dermal blood vessel shows perivascular inflammation and fibrin within blood vessels (arrow). Caspase 3 IHC (magnification of ×100) staining of the tracheobronchial lymph node on days 3 (G), 5 (H), 7 (I), and 9 (J) p.e. illustrate the progressive and profound apoptosis of lymphocytes in the germinal centers of lymphoid follicles. Caspase 3 IHC staining (magnification of ×100) of the spleen on days 3 (K), 5 (L), and 7 (M) p.e. illustrates occasional to focal apoptosis in germinal centers of splenic corpuscles that progress to diffuse apoptosis on day 9 p.e. (N).

study suggests that the rhesus macaque model of MARV infection effectively recapitulates human disease.

Valuable comparisons can be made between the aerosol sequential sacrifice study presented here, an intramuscular (i.m.) challenge serial sampling study using the less virulent MARV Ci67 (17) strain, and an aerosol challenge natural history study using MARV Angola (13, 28). Trends in tissue virus load (via plaque assay) were similar in all three studies. All of the studies found that lymphoid tissue, liver, and spleen are among the earliest infected tissues. Additionally, the viral loads in these tissues reached comparable levels regardless of the route of exposure.

Circulating infectious virus was detectable in the i.m. model with MARV strain Ci67 on days 3 to 4 p.e. in a previous study (17), while circulating infectious virus could not be recovered from both sets of MARV Angola aerosol-infected NHPs until day 4 p.e. This slight delay in systemic virus dissemination could be attributed to the differences in exposure route, virus strain, or species of macaque infected. The viral titers in both studies were comparable beginning on day 4 p.e. and ultimately reached equivalent maxima. These data indicate that challenge via aerosol and via intramuscular exposure result in similar levels of virus replication and dissemination, despite differences in the initial replication site.

The gross pathology observed following aerosol MARV Angola challenge in this study was similar to that in the previous aerosol-challenge report (13). In both studies, the most significant findings were macular rash and lesions in the tracheobronchial lymph node and liver. Early infection of the respiratory lymphoid tissues is a hallmark of aerosol challenge observed in both cynomolgus and rhesus macaques (13, 17) and is largely absent in the i.m. challenge model. Similar to aerosol exposure of cynomolgus macaques, there were few pathological changes in the lung parenchyma itself, with the exception of respiratory lymphoid lesions (13). Lung lesions in both studies were limited to mild alveolar histiocytosis, mild congestion and edema, and occasional terminal interstitial pneumonia.

Pathological evidence of infection in the liver and spleen is consistent with prior NHP studies (13, 17). Elevated liver

TABLE 3 MARV Angola antigen immunohistochemistry results[a]

Day of group sacrifice	IHC result for: Tonsil (TALT and BALT)	Lymph node (tracheobronchial and mediastinal)	Spleen	Liver	Lung	Presence of rash on haired skin[b]
1	−	−	−	−	−	None
1	−	−	−	−	−	None
1	−	−	NA	−	−	None
3	−	+	NA	−	−	None
3	−	+	−	−	−	None
3	−	++	−	−	−	None
5	+	++	+	++	−	None
5	−	+++	++	++	+	None
5	−	+++	+	++	+	None
7	−	+++	+++	+++	+	None
7	+	+++	+++	+++	+	−
7	+	+++	+++	+++	+	−
8	+	+++	+++	+++	+	−
9	+	+++	+++	+++	+	−
9	+	+++	+++	+++	+	−

[a] −, negative; +, minimal to mild (approximately 1 to 100 positive cells per 200× field); ++, moderate (approximately 100 to 500 positive cells per 200× field); +++, marked (approximately 500+ positive cells per 200× field); TALT, trachea-associated lymphoid tissue; BALT, bronchus-associated lymphoid tissue.

[b] None means there was no rash on the skin to analyze; a minus sign means there was a rash but it was negative for IHC.

transaminases (AST and ALT) and a decline in clotting factors, albumin, and total protein by day 6 p.e. were suggestive of acute severe liver disease. Azotemia (increased BUN and CRE noted at day 8 to 9 p.e.) was presumed to be prerenal azotemia due to liver disease; however, without urine specific gravity values, this could not be confirmed. Future studies would benefit from measuring urine specific gravity to evaluate kidney function in order to confirm or refute prerenal azotemia, electrolyte evaluations, and measurement of blood gases and bicarbonate levels to evaluate acid-base status. Hematological analysis from all three studies demonstrated late-stage neutrophilia as well as the expected increase in D-dimers and clotting times.

Hensley et al. described involvement of the gastrointestinal tract in the i.m. Ci67 model, specifically pyloric and ileocecal mucosal reddening beginning on day 4 (17). Alves et al. also observed pyloric and duodenal congestion at the end of the disease course in cynomolgus macaques challenged with aerosol MARV Angola variant (13). In the current study, multisystemic congestion, vasculitis, and perivasculitis were found in all organ systems, including the gastrointestinal tract (13, 17).

Coagulopathy was noted late in infection in both the i.m. and aerosol models (17). The only notable difference in coagulopathy between the two models was that clotting times peaked in the aerosol model prior to day 7 (aPTT) and 8 (PT) before decreasing, while in the i.m. model, the clotting times for both parameters continued to increase until the last group of animals was euthanized on day 9 p.e. (13, 17). Increased clotting times, PT, and aPTT, in conjunction with declining platelets, were suggestive of coagulopathy and hemorrhage. Despite evidence of hemorrhage at the histology level, RBC and hematocrit values remained relatively constant throughout this study. This was primarily attributed to the animal's ability to compensate for blood loss. Additionally, it is likely that the severe dehydration that occurs during the disease resulted in falsely elevated values. D-dimers were produced after intravascular fibrin thrombi were degraded, suggesting intravascular coagulopathy occurring around day 6 p.e.

TABLE 2 Histopathology summary[a]

Day of group sacrifice	Sinus histiocytosis (lymph node)	Lymphocytolysis	Necrotizing lymphadenitis	Splenitis	Liver necrosis + inclusion bodies	Alveolar histiocytosis	Fibrin thrombi	Vasculitis and/or perivasculitis
1	+ (I, G)	−	−	−	−	−	−	NA
1	+ (G)	−	−	−	−	−	−	NA
1	+ (I, G)	−	−	NA	−	−	−	NA
3	+ (I)	−	−	NA	−	+	−	NA
3	+ (I)	+ (T, G, S)	−	−	−	+	−	NA
3	+ (M, G)	+ (S)	−	−	−	+	−	NA
5	+++ (T)	++ (LALT, M, S)	−	−	−	+	−	NA
5	+++ (T, M); ++ (G)	+++ (T, M); ++ (LALT, BALT, S)	++ (T, M)	−	+	+	−	NA
5	+++ (T, M); ++ (I)	+++ (T, M); ++ (LALT, S)	++ (T, M)	−	+	+	−	NA
7	+++ (T, M, I, G)	+++ (T, M, BALT, S)	+++ (T, M)	+++	++	++	+	−
7	++ (I, G)	+++ (T, M, TALT, BALT, S)	++ (I, G)	+++	++	++	+	+
7	++ (I, G)	+++ (T, M, TALT, BALT, S); ++ (I, G)	+++ (T, M)	+++	++	++	+	+
8	+++ (G)	+++ (T, M, TALT, BALT, S); ++ (I, G)	+++ (T, M); ++ (G)	+++	+++	++	+++	+
9	++ (I, G)	+++ (T, M, S); ++ (I)	+++ T, M	+++	+++	++	+++	++
9	++ (I, G)	+++ (T, M, BALT, S); ++ (I)	+++ T, M	+++	+++	++	+++	++

[a] −, negative; +, minimal to mild; ++, moderate; +++, severe to marked; I, inguinal; G, gastrointestinal mesenteric; M, mediastinal; T, tracheobronchial; S, spleen; LALT, larynx-associated lymphoid tissue; BALT, bronchusassociated lymphoid tissue; TALT, trachea-associated lymphoid tissue; NA, not available.

An unexpected finding of our studies was the apparent skewing of the immune response toward a Th2 response (Fig. 5). The shift from a Th2 response to a combined Th2 and severe Th1 cytokine response intensified in late disease (day 7 to 9 p.e.) with the upregulation of Th1 cytokines (IL-6 and IFN-γ), GM-CSF, and MIP-1α. This biphasic pattern of early Th2 cytokine expression followed by Th1 expression was observed in an isolated human case of MARV in which a spike in IL-10 expression occurred early in disease and was followed by a sharp increase in IL-6 in late-stage disease (29). Late-stage increases in Th1 cytokines have also been observed in the Ci67 model (17).

It is possible that the shift toward a Th2 cytokine response early in infection could serve as a means to downregulate the antiviral Th1 response and enhance infection and disease progression, similar to infection with vaccinia virus, influenza A virus, measles virus, and human immunodeficiency virus (30–33). MARV may promote a Th2 skew in an effort to modulate the host immune response and suppress virus clearance through the induction of Th1 response. Although a Th1 response does occur in late-stage disease, the delay in this response may provide insufficient time for the immune system to combat the infection, ultimately contributing to tissue damage and pathology.

Our study results support the following model of pathogenesis for aerosol MARV infection: aerosolized virus is inhaled into the lungs and infects alveolar macrophages in the LALT, TALT, and BALT. Infected alveolar macrophages transport the virus to the mediastinal and tracheobronchial lymph nodes. Infection spreads to blood monocytes, which promote viral dissemination to other organs, including liver, spleen, blood vessels, and skin. Alterations in cytokine expression indicate an early Th2 response which shifts to a combined Th2 and severe Th1 response late in disease. The late-stage disease observed in this study recapitulates many of the clinical features of late-stage disease in human MARV infections. These results, along with complementary work describing characterization of the transcriptomes of the immune response to infection (20), provide valuable insight into the pathogenesis of and the immune response to MARV infection. In addition, this study provides a well-characterized animal model of aerosol MARV infection for the evaluation of potential prophylactics and vaccines.

ACKNOWLEDGMENTS

We gratefully acknowledge Laura Bollinger and Sandra Bixler for technical writing services; the numerous contributions of Pathology Division laboratory personnel, including Neil Davis, Phil Fogle, Gale Krietz, and Christine Mech; Calli Rooney for plaque assay analysis; and Center for Aerobiology personnel.

This research was funded by TMTI under USAMRIID project number 195732.

The views, opinions, and/or findings contained herein are those of the authors and should not be construed as an official Department of Army position, policy, or decision unless so designated by other documentation.

We declare that no conflicts of interest exist for the data presented in this report.

REFERENCES

1. **Kuhn JH, Dodd LE, Wahl-Jensen V, Radoshitzky SR, Bavari S, Jahrling PB.** 2011. Evaluation of perceived threat differences posed by filovirus variants. Biosecur Bioterror **9:**361–371. http://dx.doi.org/10.1089/bsp.2011.0051.
2. **Slenczka W, Klenk HD.** 2007. Forty years of Marburg virus. J Infect Dis **196**(Suppl 2)**:**S131–S135. http://dx.doi.org/10.1086/520551.
3. **Brauburger K, Hume AJ, Muhlberger E, Olejnik J.** 2012. Forty-five years of Marburg virus research. Viruses **4:**1878–1927. http://dx.doi.org/10.3390/v4101878.
4. **LeDuc JW.** 1989. Epidemiology of hemorrhagic fever viruses. Rev Infect Dis **11**(Suppl 4)**:**S730–S735. http://dx.doi.org/10.1093/clinids/11.Supplement_4.S730.
5. **Shu HL, Siegert R, Slenczka W.** 1969. The pathogenesis and epidemiology of the "Marburg-virus" infection. Ger Med Monthly **14:**7–10.
6. **Bausch DG, Nichol ST, Muyembe-Tamfum JJ, Borchert M, Rollin PE, Sleurs H, Campbell P, Tshioko FK, Roth C, Colebunders R, Pirard P, Mardel S, Olinda LA, Zeller H, Tshomba A, Kulidri A, Libande ML, Mulangu S, Formenty P, Grein T, Leirs H, Braack L, Ksiazek T, Zaki S, Bowen MD, Smit SB, Leman PA, Burt FJ, Kemp A, Swanepoel R, International S, Technical Committee for Marburg Hemorrhagic Fever Control in the Democratic Republic of the Congo.** 2006. Marburg hemorrhagic fever associated with multiple genetic lineages of virus. N Engl J Med **355:**909–919. http://dx.doi.org/10.1056/NEJMoa051465.
7. **Towner JS, Khristova ML, Sealy TK, Vincent MJ, Erickson BR, Bawiec DA, Hartman AL, Comer JA, Zaki SR, Stroher U, Gomes da Silva F, del Castillo F, Rollin PE, Ksiazek TG, Nichol ST.** 2006. Marburgvirus genomics and association with a large hemorrhagic fever outbreak in Angola. J Virol **80:**6497–6516. http://dx.doi.org/10.1128/JVI.00069-06.
8. **Kuhn JH.** 2008. Filoviruses. A compendium of 40 years of epidemiological, clinical, and laboratory studies. Arch Virol Suppl **20:**13–360.
9. **Ligon BL.** 2005. Outbreak of Marburg hemorrhagic fever in Angola: a review of the history of the disease and its biological aspects. Sem Pediatr Infect Dis **16:**219–224. http://dx.doi.org/10.1053/j.spid.2005.05.001.
10. **Weingartl HM, Embury-Hyatt C, Nfon C, Leung A, Smith G, Kobinger G.** 2012. Transmission of Ebola virus from pigs to non-human primates. Sci Rep **2:**811. http://dx.doi.org/10.1038/srep00811.
11. **Piercy TJ, Smither SJ, Steward JA, Eastaugh L, Lever MS.** 2010. The survival of filoviruses in liquids, on solid substrates and in a dynamic aerosol. J Appl Microbiol **109:**1531–1539. http://dx.doi.org/10.1111/j.1365-2672.2010.04778.x.
12. **U.S. Food and Drug Administration.** 2002. New drug and biological drug products; evidence needed to demonstrate effectiveness of new drugs when human efficacy studies are not ethical or feasible. Final rule. Fed Reg **67:**37988–37998.
13. **Alves DA, Glynn AR, Steele KE, Lackemeyer MG, Garza NL, Buck JG, Mech C, Reed DS.** 2010. Aerosol exposure to the angola strain of marburg virus causes lethal viral hemorrhagic Fever in cynomolgus macaques. Vet Pathol **47:**831–851. http://dx.doi.org/10.1177/0300985810378597.
14. **Nakayama E, Saijo M.** 2013. Animal models for Ebola and Marburg virus infections. Front Microbiol **4:**267. http://dx.doi.org/10.3389/fmicb.2013.00267.
15. **Bente D, Gren J, Strong JE, Feldmann H.** 2009. Disease modeling for Ebola and Marburg viruses. Dis Model Mech **2:**12–17. http://dx.doi.org/10.1242/dmm.000471.
16. **Geisbert TW, Daddario-DiCaprio KM, Geisbert JB, Young HA, Formenty P, Fritz EA, Larsen T, Hensley LE.** 2007. Marburg virus Angola infection of rhesus macaques: pathogenesis and treatment with recombinant nematode anticoagulant protein c2. J Infect Dis **196**(Suppl 2)**:**S372–S381. http://dx.doi.org/10.1086/520608.
17. **Hensley LE, Alves DA, Geisbert JB, Fritz EA, Reed C, Larsen T, Geisbert TW.** 2011. Pathogenesis of Marburg hemorrhagic fever in cynomolgus macaques. J Infect Dis **204**(Suppl 3)**:**S1021–S1031. http://dx.doi.org/10.1093/infdis/jir339.
18. **Murphy FA, Simpson DI, Whitfield SG, Zlotnik I, Carter GB.** 1971. Marburg virus infection in monkeys. Ultrastructural studies. Lab Invest **24:**279–291.
19. **Simpson DI.** 1969. Marburg agent disease: in monkeys. Trans R Soc Trop Med Hyg **63:**303–309. http://dx.doi.org/10.1016/0035-9203(69)90002-9.
20. **Connor JH, Yen J, Caballero IS, Garamszegi S, Malhotra S, Lin K, Hensley L, Goff A.** 2015. Transcriptional profiling of the immune response to Marburg virus infection. J Virol **89:**9865–9874. http://dx.doi.org/10.1128/JVI.01142-15.
21. **National Research Council.** 2011. Guide for the care and use of laboratory animals, 8th ed. National Academies Press, Washington, DC.
22. **Trombley AR, Wachter L, Garrison J, Buckley-Beason VA, Jahrling J, Hensley LE, Schoepp RJ, Norwood DA, Goba A, Fair JN, Kulesh DA.** 2010. Comprehensive panel of real-time TaqMan polymerase chain reaction assays for detection and absolute quantification of filoviruses, arenaviruses, and New World hantaviruses. Am J Trop Med Hyg **82:**954–960. http://dx.doi.org/10.4269/ajtmh.2010.09-0636.

23. **Hartman AL, Towner JS, Nichol ST.** 2010. Ebola and marburg hemorrhagic fever. Clin Lab Med **30:**161–177. http://dx.doi.org/10.1016/j.cll.2009.12.001.
24. **Mehedi M, Groseth A, Feldmann H, Ebihara H.** 2011. Clinical aspects of Marburg hemorrhagic fever. Future Virol **6:**1091–1106. http://dx.doi.org/10.2217/fvl.11.79.
25. **Kortepeter MG, Bausch DG, Bray M.** 2011. Basic clinical and laboratory features of filoviral hemorrhagic fever. J Infect Dis **204**(Suppl 3)**:**S810–S816. http://dx.doi.org/10.1093/infdis/jir299.
26. **Mohamadzadeh M, Chen L, Schmaljohn AL.** 2007. How Ebola and Marburg viruses battle the immune system. Nat Rev Immunol **7:**556–567. http://dx.doi.org/10.1038/nri2098.
27. **Bausch DG, Sprecher AG, Jeffs B, Boumandouki P.** 2008. Treatment of Marburg and Ebola hemorrhagic fevers: a strategy for testing new drugs and vaccines under outbreak conditions. Antivir Res **78:**150–161. http://dx.doi.org/10.1016/j.antiviral.2008.01.152.
28. **Daddario-DiCaprio KM, Geisbert TW, Geisbert JB, Stroher U, Hensley LE, Grolla A, Fritz EA, Feldmann F, Feldmann H, Jones SM.** 2006. Cross-protection against Marburg virus strains by using a live, attenuated recombinant vaccine. J Virol **80:**9659–9666. http://dx.doi.org/10.1128/JVI.00959-06.
29. **van Paassen J, Bauer MP, Arbous MS, Visser LG, Schmidt-Chanasit J, Schilling S, Olschlager S, Rieger T, Emmerich P, Schmetz C, van de Berkmortel F, van Hoek B, van Burgel ND, Osterhaus AD, Vossen AC, Gunther S, van Dissel JT.** 2012. Acute liver failure, multiorgan failure, cerebral oedema, and activation of proangiogenic and antiangiogenic factors in a case of Marburg haemorrhagic fever. Lancet Infect Dis **12:**635–642. http://dx.doi.org/10.1016/S1473-3099(12)70018-X.
30. **van Den Broek M, Bachmann MF, Kohler G, Barner M, Escher R, Zinkernagel R, Kopf M.** 2000. IL-4 and IL-10 antagonize IL-12-mediated protection against acute vaccinia virus infection with a limited role of IFN-gamma and nitric oxide synthetase 2. J Immunol **164:**371–378. http://dx.doi.org/10.4049/jimmunol.164.1.371.
31. **Sharma DP, Ramsay AJ, Maguire DJ, Rolph MS, Ramshaw IA.** 1996. Interleukin-4 mediates down regulation of antiviral cytokine expression and cytotoxic T-lymphocyte responses and exacerbates vaccinia virus infection in vivo. J Virol **70:**7103–7107.
32. **Carsillo M, Klapproth K, Niewiesk S.** 2009. Cytokine imbalance after measles virus infection has no correlation with immune suppression. J Virol **83:**7244–7251. http://dx.doi.org/10.1128/JVI.00148-09.
33. **Lee S, Almeida CA, French MA, Price P.** 2004. Persistent HIV-1 replication does not explain low levels of T-cell interferon gamma mRNA and elevated serum NO_2^-/NO_3^- in patients with stable CD4 T-cell responses to HAART. Clin Exp Immunol **138:**110–115. http://dx.doi.org/10.1111/j.1365-2249.2004.02589.x.